Empirical Models of the Probability Distribution of Sea Surface Wind Speeds

ADAM HUGH MONAHAN

School of Earth and Ocean Sciences, University of Victoria, Victoria, British Columbia, and Earth Systems Evolution Program, Canadian Institute for Advanced Research, Toronto, Ontario, Canada

(Manuscript received 27 July 2006, in final form 23 February 2007)

ABSTRACT

This study considers the probability distribution of sea surface wind speeds, which have historically been modeled using the Weibull distribution. First, non-Weibull structure in the observed sea surface wind speeds (from SeaWinds observations) is characterized using relative entropy, a natural information theoretic measure of the difference between probability distributions. Second, empirical models of the probability distribution of sea surface wind speeds, parameterized in terms of the parameters of the vector wind probability distribution, are developed. It is shown that Gaussian fluctuations in the vector wind cannot account for the observed features of the sea surface wind speed distribution, even if anisotropy in the fluctuations is accounted for. Four different non-Gaussian models of the vector wind distribution are then considered: the bi-Gaussian, the centered gamma, the Gram–Charlier, and the constrained maximum entropy. It is shown that so long as the relationship between the skewness and kurtosis of the along-mean sea surface wind component characteristic of observations is accounted for in the modeled probability distribution, then all four vector wind distributions are able to simulate the observed mean, standard deviation, and skewness of the sea surface wind speeds with an accuracy much higher than is possible if non-Gaussian structure in the vector winds is neglected. The constrained maximum entropy distribution is found to lead to the best simulation of the wind speed probability distribution. The significance of these results for the parameterization of air/sea fluxes in general circulation models is discussed.

1. Introduction

Air/sea fluxes of mass, momentum, and energy are mediated by the character of turbulence in both the atmospheric and oceanic boundary layers. In particular, the surface turbulent momentum flux is affected by and feeds back on sea surface wind speeds, where in this study the term "sea surface wind" will refer to the eddy-averaged wind at the standard anemometer height of 10 m. Wind shears drive the boundary layer turbulence, which in turn determines the rate at which momentum is exchanged with the upper ocean. Because surface fluxes generally have a nonlinear dependence on the sea surface wind speed, the area- or time-averaged fluxes are not equal to the fluxes diagnosed from the averaged winds. This fact is of potential importance to the calculation of air/sea fluxes in general circulation models (GCMs), in which only gridbox averaged vector winds are available to calculate gridbox-averaged fluxes (e.g., Cakmur et al. 2004). Calculation of the spatially averaged fluxes requires knowledge of wind speed moments of higher order than the mean; in fact, there is value to having the entire probability density function (pdf). Furthermore, the gridbox-averaged wind speed will not generally equal the magnitude of the gridbox-averaged vector wind; it is easy to show that higher-order moments of the vector winds will influence the mean wind speed (e.g., Mahrt and Sun 1995). This motivates the need for developing parameterizations of sea surface wind pdfs that take as input grid-scale-resolved variables, in particular moments of the vector winds. Improved parameterizations of sea surface wind speed pdfs are also relevant to improving observational diagnoses of air/sea fluxes (e.g., Wanninkhof 1992; Wanninkhof and McGillis 1999; Taylor 2000; Wanninkhof et al. 2002). Note that we are assuming spatial stationarity of surface wind statistics on the gridbox scale, so probability distributions in space and in time are interchangeable. That is, we assume that collocated individual observations of the wind taken at different times will follow the same distribution as simultaneous

Corresponding author address: Adam Hugh Monahan, School of Earth and Ocean Sciences, University of Victoria, P.O. Box 3055 STN CSC, Victoria, BC V8P 5C2, Canada.
E-mail: monahana@uvic.ca

DOI: 10.1175/2007JCLI1609.1

individual observations of the wind taken at different locations (on scales where boundary conditions are homogeneous). This assumption is analogous to a weak version of Taylor's "frozen turbulence" hypothesis (weak because it is applied to the marginal distributions of the wind field, not full joint distributions).

The beginnings of a systematic theory for the probability distribution of sea surface wind speeds were presented in Monahan (2006a). In this earlier study, it was shown that the moments of wind speed are functionally related: the skewness is a decreasing, concave upward function of the ratio of the mean to the standard deviation, such that the skewness is positive when this ratio is small, near zero where the ratio is intermediate, and negative when the ratio is large. This relationship, which is shared with the Weibull distribution traditionally used to parameterize surface wind speed pdfs, was shown to follow from elementary boundary layer physics. In particular, the fact that the wind speed skewness can become negative was demonstrated to be a consequence of skewness in the vector winds resulting from the nonlinear dependence of surface drag on wind speed (Monahan 2004b). These facts were used to construct empirical parameterizations of sea surface vector wind and wind speed pdfs, using Gram–Charlier expansions of a Gaussian (e.g., Johnson et al. 1994) to produce along-mean wind component distributions with nonzero skewness and kurtosis. While this approach was able to demonstrate the importance of simulating the pdf of sea surface wind speeds of non-Gaussian structure in the vector winds, the Gram–Charlier distribution is problematic in that it is not guaranteed to be positive-definite (e.g., Johnson et al. 1994; Jondeau and Rockinger 2001). This is theoretically unsatisfactory and practically limiting in that the associated random variable is not realizable.

The present study has two primary goals. The first is to further characterize the deviations in observed sea surface wind pdfs from Weibull structure discussed in Monahan (2006a,b) through the use of relative entropy, a natural metric for the difference between probability distributions. Second, and more significantly, the present study further develops empirical parameterizations of sea surface wind speed pdfs in terms of moments of the vector winds. The importance of anisotropic fluctuations in vector winds is first considered, and then the wind speed pdf parameterizations arising from four different non-Gaussian distributions of the vector winds are compared. Section 2 of this study describes the dataset used in the analysis and establishes notation. Deviations of observed sea surface wind speed pdfs from the Weibull distribution are characterized and discussed in section 3. The empirical sea surface wind speed pdf parameterizations are developed and assessed in section 4, and a discussion and conclusions are presented in section 5.

2. Data

The sea surface wind dataset considered in this study consists of level-3.0 gridded daily SeaWinds scatterometer 10-m zonal and meridional wind observations from the National Aeronautics and Space Administration Quick Scatterometer (NASA QuikSCAT) satellite (Jet Propulsion Laboratory 2001), available on a $1/4^\circ \times 1/4^\circ$ grid from 19 July 1999 to the present (31 December 2005 for the present study). These data are available to download from the NASA Jet Propulsion Laboratory (JPL) Distributed Active Archive Center (http://podaac.jpl.nasa.gov). The SeaWinds data have been extensively compared with buoy and ship measurements of surface winds (Ebuchi et al. 2002; Bourassa et al. 2003; Chelton and Freilich 2005); the root-mean-squared errors of the remotely sensed wind speed and direction are both found to depend on wind speed, with average values of ~ 1 m s^{-1} and $\sim 20^\circ$, respectively. Because raindrops are effective scatterers of microwaves in the wavelength band used by the SeaWinds scatterometer, rainfall can lead to errors in estimates of sea surface winds. The SeaWinds level-3.0 dataset flags those data points that are estimated as likely to have been corrupted by rain (Jet Propulsion Laboratory 2001); these data points have been excluded from the present analysis.

No further processing of the data, such as filtering or removing the annual cycle, was carried out on this dataset. There is significant seasonal variability in the probability distributions of both vector winds and wind speeds (Monahan 2006b); the data analyzed in this study were not seasonally stratified because of the relatively short duration of the SeaWinds dataset. The analysis has been repeated with 6-hourly National Centers for Environmental Prediction–National Center for Atmospheric Research (NCEP–NCAR) reanalysis 10-m winds, which span the much longer period from 1 January 1948 to the present. Differences between the statistical structure of SeaWinds and NCEP–NCAR sea surface winds were considered in Monahan (2006b), in which it was shown that while the moment fields of the two datasets agree to leading order, they display some regional differences in detail (particularly over the Southern Ocean and Tropics). The results of the analysis carried out using the NCEP–NCAR data are qualitatively the same as those reported in the following sections. Because the SeaWinds data are a more direct representation of observed sea surface winds than re-

analysis products (which are a hybrid of observations and general circulation model output), they were chosen as the dataset on which this study will focus.

In this study, we will consider surface wind vector components defined relative to a local coordinate system. The notation we use is u = wind component along local time-mean wind vector, v = wind component across local time-mean wind vector (positive to the left), $\mathbf{u} = (u, v)$ wind vector, and w = wind speed.

The use of a local coordinate system does not lead to any computational difficulties in this study, as only single-point statistics are considered.

The present study makes frequent use of the skewness and kurtosis of the sea surface vector winds and wind speeds; for a random variable x, these quantities are defined, respectively, as the normalized third- and fourth-order moments:

$$\text{skew}(x) = \frac{\text{mean}\{[x - \text{mean}(x)]^3\}}{\text{std}^3(x)}, \tag{1}$$

$$\text{kurt}(x) = \frac{\text{mean}\{[x - \text{mean}(x)]^4\}}{\text{std}^4(x)} - 3, \tag{2}$$

where std is the standard deviation. Both of these quantities are zero for Gaussian random variables.

3. Sea surface wind speed pdfs: Observations

The first row of Fig. 1 displays the fields of mean(w), std(w), and skew(w) estimated from SeaWinds observations. The mean(w) field is characterized by high values in the extratropics, secondary maxima along the equatorward flanks of the subtropical highs, and minima in the equatorial doldrums and subtropical horse latitudes. Maxima in std(w) occur in the midlatitude storm tracks, while values in the subtropics and Tropics are generally small. Finally, skew(w) is positive in the NH midlatitudes and between the bands of westerlies and easterlies in the SH, it is near zero around the Southern Ocean, and it is negative throughout most of the Tropics. A detailed discussion of these fields and their physical origin is given in Monahan (2006a).

Historically, wind speed pdfs have been parameterized using the two-parameter Weibull distribution (e.g., Hennessey 1977; Justus et al. 1978; Conradsen et al. 1984; Pavia and O'Brien 1986; Isemer and Hasse 1991; Deaves and Lines 1997; Pang et al. 2001), although it has been noted that the fit is not exact (e.g., Stewart and Essenwanger 1978; Takle and Brown 1978; Tuller and Brett 1984; Erickson and Taylor 1989; Bauer 1996). Deviations of observed wind speed pdfs from Weibull structure were discussed in Monahan (2006a,b) in terms of differences between observed moments (mean, standard deviation, and skewness) and those of the best-fit Weibull distributions. A more comprehensive measure of the difference between two probability distributions, $p_1(x)$ and $p_2(x)$, is their relative entropy:

$$\rho(p_1 \| p_2) = \int p_1 \ln\left(\frac{p_1}{p_2}\right) dx \tag{3}$$

(e.g., Kleeman 2002, 2006; Kleeman and Majda 2005). Although it is nonnegative, the relative entropy is not a Euclidean distance measure [in particular, it is not commutative: $\rho(p_1 \| p_2) \neq \rho(p_2 \| p_1)$]. Nevertheless, relative entropy is a useful metric of the difference between probability distributions. In particular, the relative entropy between a given pdf and the Gaussian with the same covariance matrix has been used as a measure of non-Gaussianity (e.g., Abramov et al. 2005). In a comparable fashion, we will consider the relative entropy between the observed sea surface wind speed pdf, $p_w(w)$, and the Weibull distribution with the best-fit parameters, $p_{\text{wbl}}(w)$, as a measure of non-Weibull structure; a map of estimated $\rho(p_w \| p_{\text{wbl}})$ is given in Fig. 2. Algorithms for the estimation of relative entropy are an active field of research (e.g., Kleeman and Majda 2005; Haven et al. 2005); the estimates presented in Fig. 2 were obtained by first calculating the maximum entropy distribution constrained by the wind speed mean, standard deviation, skewness, and kurtosis (section e of appendix B), and then numerically integrating Eq. (3). The solid black contour in Fig. 2 is the 95% confidence level for the null hypothesis that the observed relative entropy arises due to sampling fluctuations from an underlying Weibull distribution. This value was calculated to be $\rho = 6 \times 10^{-3}$ from a Monte Carlo simulation assuming the wind dataset consisted of 1000 statistical degrees of freedom (5.5 yr of daily data with an approximately 2-day autocorrelation e-folding time; Monahan 2004b).

Statistically significant deviations from Weibull structure are evident throughout the Tropics and in the NH midlatitudes, consistent with the skewness difference field illustrated in Monahan (2006a). The best-fit Weibull pdf at a typical midlatitude point [30°N, 165°W, where $\rho(p_1 \| p_2) = 0.013$] is compared to a kernel density estimate (Silverman 1986) of the observed wind speed in Fig. 3. While the two pdfs are not dramatically different, the observed wind speed pdf is narrower with a longer tail and more positive skewness than the corresponding Weibull pdf. Non-Weibull structure in surface wind speed pdfs is modest but robust and widespread, motivating the characterization of sea surface wind speeds pdfs that are more accurate than the

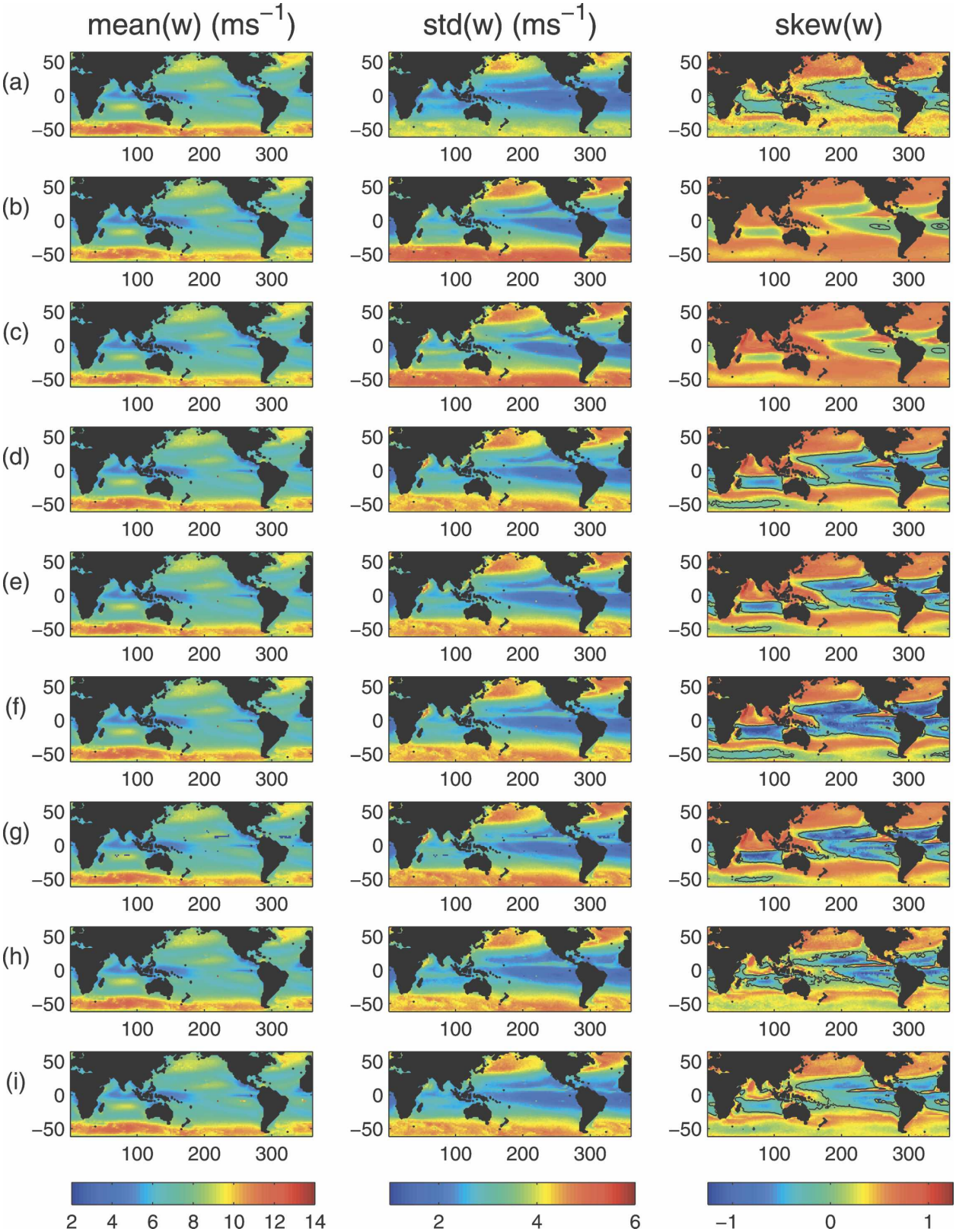

FIG. 1. Maps of mean(w), std(w), and skew(w) from (a) SeaWinds observations, (b) the isotropic Gaussian model, (c) the anisotropic Gaussian model, (d) the bi-Gaussian model, (e) the centered gamma model, (f) the Gram–Charlier model with kurt(u) = 0, (g) the constrained maximum entropy model with kurt(u) = 0, (h) the Gram–Charlier model with observed kurt(u), and (i) the constrained maximum entropy model with observed kurt(u).

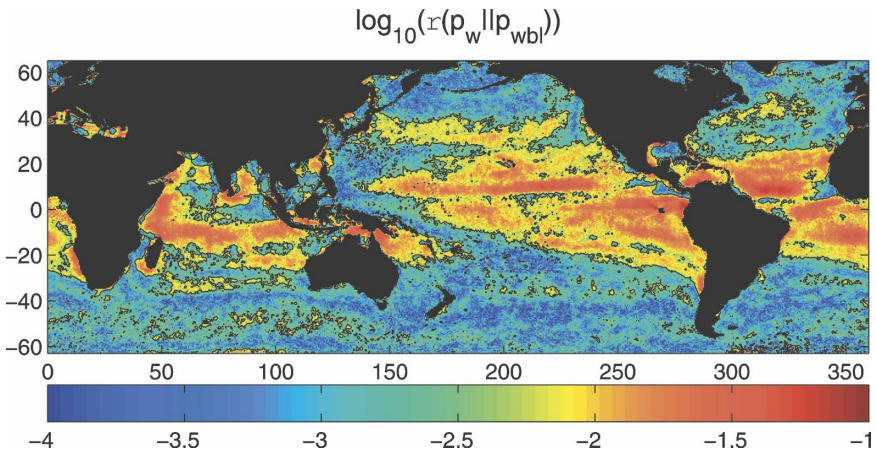

FIG. 2. Global estimates of the relative entropy $\rho(p_w \| p_{\mathrm{wbl}})$ between the observed wind speed pdfs and the best-fit Weibull distributions. The black contour denotes the 95% confidence level, as described in the text.

Weibull distribution. Furthermore, the Weibull distribution is specified in terms of parameters (the shape and scale parameters; see section a of appendix B) that are not directly related to the grid-scale quantities produced by GCMs. In the next section, we will develop parameterizations of the sea surface wind speed that are of greater fidelity to nature than the Weibull distribution and use as input information moments of the sea surface vector winds.

4. Sea surface wind speed pdfs: Empirical models

The primary goal of this study is the development of parameterizations of wind speed pdfs that take as input moments of the vector winds; a natural place to start is the derivation of the wind speed pdf from the vector wind pdf. Given the joint pdf $p_{uv}(u, v)$ of the vector wind, the wind speed pdf $p_w(w)$ can be obtained through a change to polar coordinates and an integration over wind direction:

$$p_w(w) = w \int_{-\pi}^{\pi} p_{uv}(w \cos\theta, w \sin\theta)\, d\theta, \tag{4}$$

where the factor of w before the integral comes from the Jacobian of the coordinate transformation as required by conservation of probability. This calculation can be simplified by assuming that (i) the vector wind components u and v are independent so their joint distribution factors as the product of the marginals:

$$p_{uv}(u, v) = p_u(u) p_v(v), \tag{5}$$

and (ii) that the distribution of v is Gaussian:

$$p_v(v) = \frac{1}{\sqrt{2\pi\sigma_v^2}} \exp\left(-\frac{v^2}{2\sigma_v^2}\right) \tag{6}$$

[where by definition mean$(v) = 0$]. Then

$$p_w(w) = \frac{w}{\sqrt{2\pi\sigma_v^2}} \int_{-\pi}^{\pi} p_u(w \cos\theta) \exp\left(-\frac{w^2 \sin^2\theta}{2\sigma_v^2}\right) d\theta. \tag{7}$$

Different parameterizations of $p_w(w)$ then follow from different models of the pdf of the along-mean wind component u.

It was demonstrated in Monahan (2004b) that the sea surface vector winds are non-Gaussian, such that the mean and skewness fields are anticorrelated for both

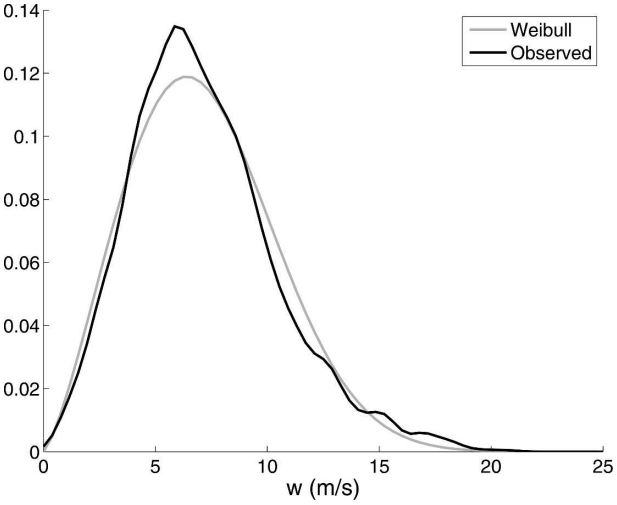

FIG. 3. Best-fit Weibull pdf (gray line) and Gaussian kernel density pdf estimate (black line) for wind speeds at (30°N, 165°W).

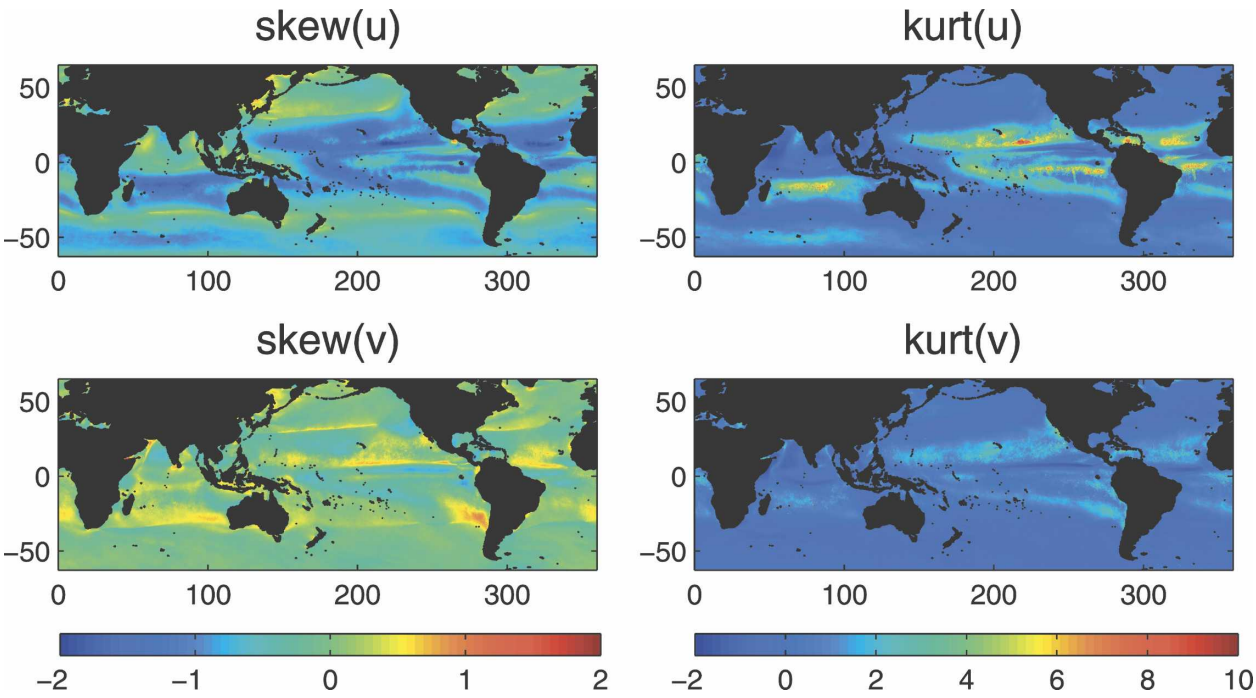

FIG. 4. Skewness and kurtosis fields for the along-mean wind component u and the cross-mean wind component v.

the zonal and meridional components. This relationship between moments was demonstrated to follow from the nonlinear dependence of surface drag on sea surface wind speed. Maps of the skewness and kurtosis fields estimated from the SeaWinds data for the along- and cross-mean wind components are presented in Fig. 4. It is evident that the distribution of the along-mean wind component displays non-Gaussian structure, with strongly negative skewness in both the Tropics and the Southern Ocean, where mean(u) is strongly positive [note that mean(u) is positive by definition], and strongly positive kurtosis in the Tropics. Deviations of the distribution of v from Gaussianity are considerably weaker: skew(v) is nonzero in the subtropical highs and along the ITCZ, but the magnitudes are considerably smaller than those of skew(u). Similarly, kurt(v) takes positive values in the Tropics, but much less so than kurt(u). Thus, while u is strongly non-Gaussian, the approximation that v has a Gaussian distribution is reasonable to first order.

The statistical dependence of u and v was discussed in Monahan (2006a); Fig. 5 displays a plot of the squared correlation coefficient between u and v (the fraction of variance accounted for by a linear relation between u and v). Clearly, linear dependence between the along- and cross-wind components is weak, except over the equatorial oceans and monsoon regions where seasonal variability is strong. Of course, a vanishing correlation coefficient does not imply independence unless the joint distribution of u and v is Gaussian. The stochastic boundary layer model in Monahan (2006a) predicts that u and v should be uncorrelated but not independent. A more general measure of dependence employs the mutual information,

$$\mathcal{M}(u, v) = \int p_{uv}(u, v) \ln\left[\frac{p_{uv}(u, v)}{p_u(u)p_v(v)}\right] du\, dv, \qquad (8)$$

defined as the relative entropy between the joint distribution $p_{uv}(u, v)$ and the product of the marginals $p_u(u)p_v(v)$; this quantity vanishes only if the joint distribution factors as the product of its marginals, that is, when u and v are independent [Eq. (5)]. The quantity

$$C^2 = 1 - \exp[-2\mathcal{M}(u, v)] \qquad (9)$$

varies between 0 (u, v independent) and 1 (u, v perfectly dependent) and is equal to the squared correlation coefficient between u and v when $p_{uv}(u, v)$ is Gaussian; C^2 is a non-Gaussian generalization of the squared correlation coefficient. A map of C^2 (not shown) is not significantly different from the map of the squared correlation coefficient in Fig. 5, indicating that while u displays significant non-Gaussian structure, the covariability between u and v is not strongly nonlinear. Thus, while the assumption of independence of u and v is violated in a few localized regions, it is not a bad approximation on a global scale and it considerably sim-

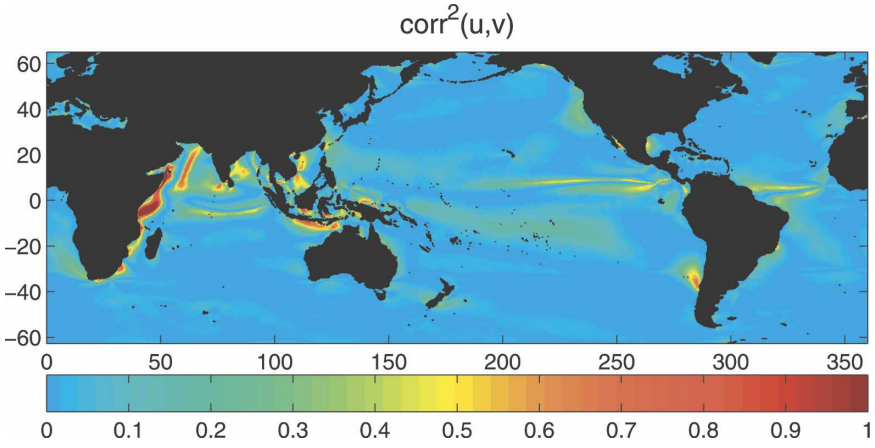

FIG. 5. Square of the correlation coefficient between the along- and cross-mean wind components (u and v) of the sea surface vector winds; this quantity is the fraction of variance accounted for by a linear relationship between the two variables.

plifies the computation of the wind speed pdf from the pdf of vector winds.

We will now proceed to develop several different wind speed pdf parameterizations $p_w(w)$ following from different models for the pdf of the along-mean wind component, $p_u(u)$. The accuracy of these pdfs will be assessed by comparing the fields of mean(w), std(w), and skew(w) simulated using the fields of the vector wind moments estimated from the SeaWinds data to the observed wind speed moment fields.

a. Gaussian fluctuations in u

While it is evident from Fig. 4 that the distribution of u is non-Gaussian, to assess the importance of this non-Gaussian structure to the pdf of w we first consider the structure of $p_w(w)$ following from Gaussian $p_u(u)$. The case of isotropic Gaussian winds,

$$p_u(u) = \frac{1}{\sqrt{2\pi\sigma_u^2}} \exp\left[-\frac{(u-\overline{u})^2}{2\sigma_u^2} \right] \tag{10}$$

with $\sigma_u = \sigma_v = \sigma$, was considered in Cakmur et al. (2004) and Monahan (2006a); the integral in Eq. (7) can be evaluated to yield

$$p_w(w) = \frac{w}{\sigma^2} \exp\left(-\frac{w^2 + \overline{u}^2}{2\sigma^2} \right) I_0\left(\frac{\overline{u}w}{\sigma^2} \right), \tag{11}$$

where $I_0(z)$ is the zeroth-order associated Bessel function of the first kind (Gradshteyn and Ryzhik 2000). The second row of Fig. 1 displays maps of the mean(w), std(w) and skew(w) fields following from the pdf (11); the first row of Fig. 6 displays the differences between these modeled fields and those estimated from SeaWinds observations. The isotropic standard deviation σ was calculated from observations as

$$\sigma = \sqrt{\frac{1}{2}[\mathrm{std}^2(u) + \mathrm{std}^2(v)]}\ . \tag{12}$$

As was discussed in Monahan (2006a), the speed pdf following from isotropic Gaussian fluctuations in the vector wind underestimates mean(w) and overestimates std(w) relative to observations (except in the Tropics and the North Pacific) and has a positive bias in skew(w) throughout the Tropics and over much of the Southern Ocean. In particular, the pdf (11) cannot characterize the negative skew(w) in the Tropics and the band of near-zero skew(w) over the Southern Ocean.

The observed pdf of sea surface wind speeds is characterized by a distinct relationship between the moments: skew(w) is a strong function of the ratio mean(w)/std(w), such that the skewness is positive where the ratio is small, near zero where the ratio is intermediate, and negative where the ratio is large. This relationship between moments is also characteristic of the Weibull distribution. Figure 7 displays a Gaussian kernel estimate of the observed joint distribution of mean(w)/std(w) with skew(w) along with a scatterplot of these fields simulated by the model pdf (11). As is discussed in Monahan (2006a), the relationship between wind speed moments following from the assumption of isotropic Gaussian fluctuations in the vector wind falls within the observed relationship for regions of weak mean wind speed or large wind speed variability but is unable to capture this relationship for larger values of the ratio mean(w)/std(w).

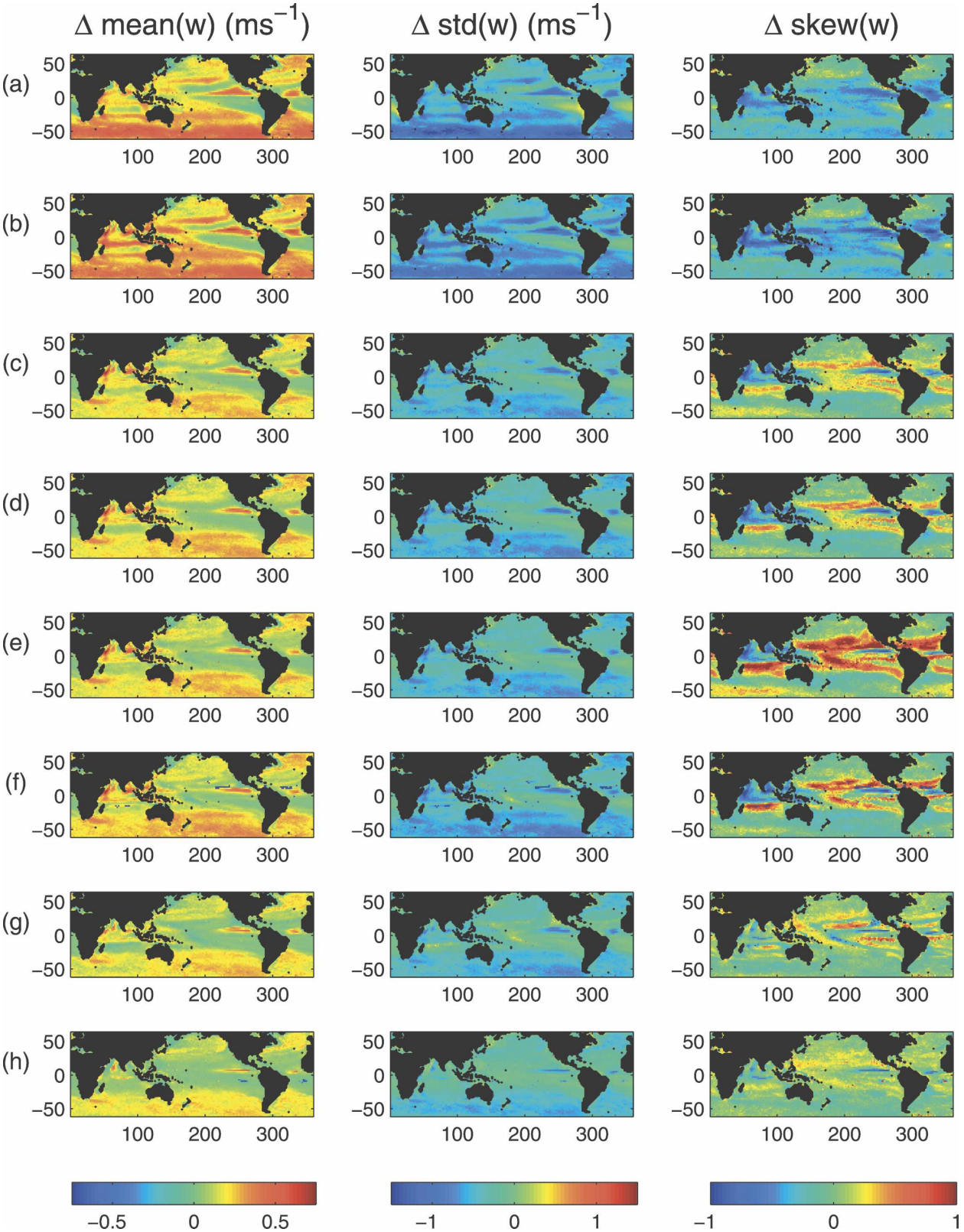

FIG. 6. Maps of the difference fields between observed and modeled (observed − modeled) mean(w), std(w), and skew(w) from (a) the isotropic Gaussian model, (b) the anisotropic Gaussian model, (c) the bi-Gaussian model, (d) the centered gamma model, (e) the Gram–Charlier model with kurt(u) = 0, (f) the constrained maximum entropy model with kurt(u) = 0, (g) the Gram–Charlier model with observed kurt(u), and (h) the constrained maximum entropy model with observed kurt(u).

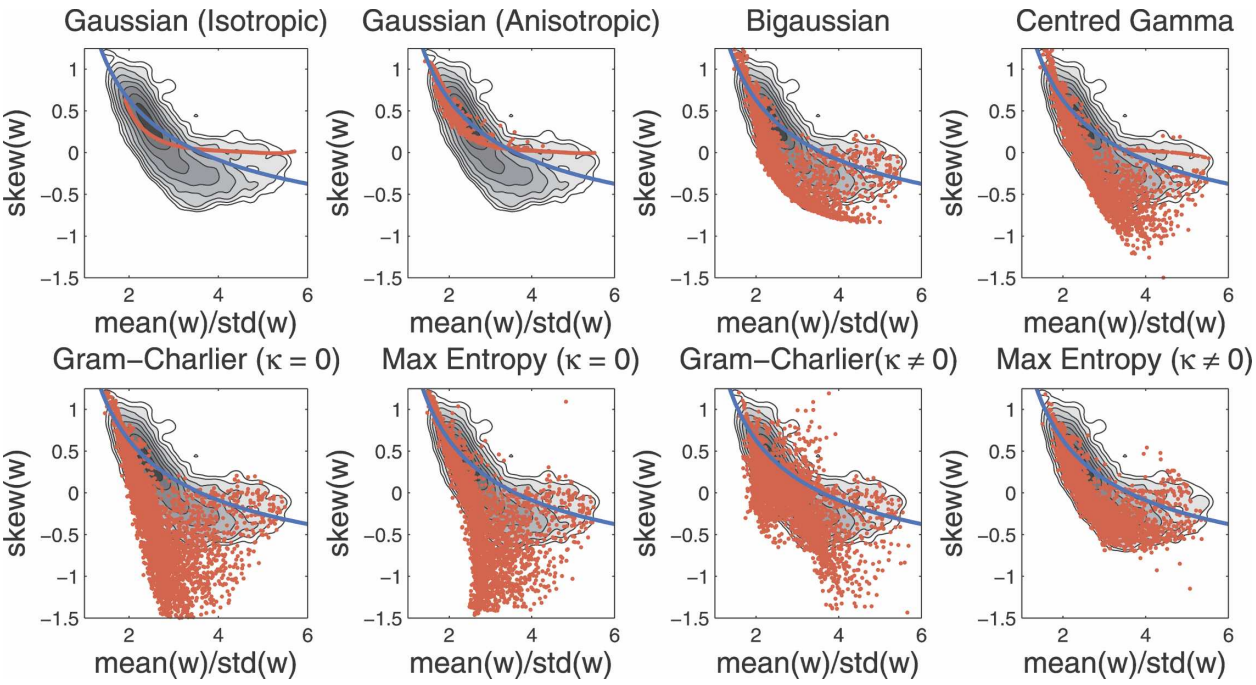

FIG. 7. Relationship between the ratio mean(w)/std(w) and skew(w). Shaded contours represent the kernel density estimate of the relationship from SeaWinds observations; blue line represents the relationship for the Weibull distribution; red dots represent relationships for the different parameterizations of the pdf of w. In the second row, κ = kurt(u).

Clearly, isotropic Gaussian fluctuations in the vector wind are not consistent with observed distributions of sea surface wind speeds. These biases may arise because of the assumption of isotropic vector wind fluctuations; to test this, the integral (7) was evaluated with $p_u(u)$ given by Eq. (10) with $\sigma_u \neq \sigma_v$. The integral for $p_w(w)$ can be evaluated as the infinite series of Bessel functions:

$$p_w(w) = \frac{w}{\sqrt{\pi\sigma_u\sigma_v}} \exp\left(-\frac{w^2+\overline{u}^2}{2\sigma_u^2}\right) \sum_{k=0}^{\infty} \left[\frac{w}{\overline{u}}\left(1-\frac{\sigma_u^2}{\sigma_v^2}\right)\right]^k \frac{\Gamma(k+1/2)}{k!} I_k\left(\frac{\overline{u}w}{\sigma_u^2}\right) \tag{13}$$

(see appendix A). The quantity

$$\lambda = 1 - \frac{\sigma_u^2}{\sigma_v^2} \tag{14}$$

arises as a natural anisotropy parameter; as $\lambda \to 0$ and the fluctuations become isotropic, the pdf (13) reduces to (11). The mean, standard deviation, and skewness of w calculated from Eq. (13) using observed values of mean(u), std(u), and std(v) are presented in the third row of Fig. 1; the corresponding difference maps with the observed moment fields are presented in the second row of Fig. 6. These fields are essentially the same as those of the pdf of w following from the assumption of isotropic Gaussian fluctuations. Furthermore, there is no substantial improvement on the characterization of the relationship between the ratio mean(w)/std(w) and skew(w) (Fig. 7). Evidently, no improvement in the parameterization of the wind speed pdf follows from accounting for anisotropy in the Gaussian vector wind fluctuations. In fact, as illustrated in Fig. 4, the vector winds are manifestly non-Gaussian. We now proceed to consider the importance for parameterizing the pdf of wind speeds of accounting for non-Gaussian structure in the vector winds.

b. *Non-Gaussian fluctuations in u: Specifying skewness*

We first consider the importance for simulation of the sea surface wind speed pdf of accounting for skewness in the vector winds. Four pdfs in which the skewness can be specified independently from the mean and standard deviation will be considered: the bi-Gaussian distribution, the centered gamma distribution, the Gram–Charlier expansion of a Gaussian, and the con-

strained maximum entropy distribution. These distributions are discussed in detail in appendix B; all four of these distributions converge to Gaussians in the limits that skew(u) and kurt(u) are zero. The Gram–Charlier expansion of a Gaussian was considered in Monahan (2006a); as is discussed in appendix B, this quantity can take negative values and is therefore not truly a pdf (the associated random variable is not realizable). The other three distributions are true pdfs. For all distributions except the Gram–Charlier, the integral over wind direction (7) cannot be evaluated analytically and must be computed numerically. The analytic results for the Gram–Charlier distribution are presented in Monahan (2006a). For both the Gram–Charlier and constrained maximum entropy distributions, the kurtosis must be specified as well as the skewness; in this section, we will take kurt(u) = 0. For these calculations, σ_u and σ_v are assumed to be equal and given by Eq. (12).

The fields of mean(w), std(w), and skew(w) computed from SeaWinds observations of mean(u), std(u), and skew(u) are presented in the fourth through the seventh rows of Fig. 1; the associated difference fields with the SeaWinds wind speed moments are shown in the third through the sixth columns of Fig. 6. For all four distributions, the incorporation of skew(u) information improves agreement between observed and modeled fields of mean(w) and std(w). Furthermore, as in observations, modeled skew(w) is now negative throughout much of the Tropics and near zero over the Southern Ocean. For all four distributions, however, skew(w) is too strongly negative in the Tropics; this bias is particularly strong for the Gram–Charlier and constrained maximum entropy distributions. Incorporating skew(u) information into the parameterization has not eliminated the bias in the skew(w) characteristic of the distributions following from the assumption of Gaussian fluctuations in the vector wind; the sign has simply been reversed. This bias is also evident in scatterplots of mean(w)/std(w) with skew(w) (Fig. 7); for all four pdfs, while the simulated relationship between moments resembles that of observations, the simulated scatterplots fall below the observed relationship between moments. Again, this bias is particularly strong for the Gram–Charlier and constrained maximum entropy distributions.

c. *Non-Gaussian fluctuations in u: Specifying both skewness and kurtosis*

In the previous section, it was assumed (for the Gram–Charlier and constrained maximum entropy distributions) that the kurtosis of the along-mean sea surface wind component was zero. In fact, observations indicate that kurt(u) is generally nonzero and strongly

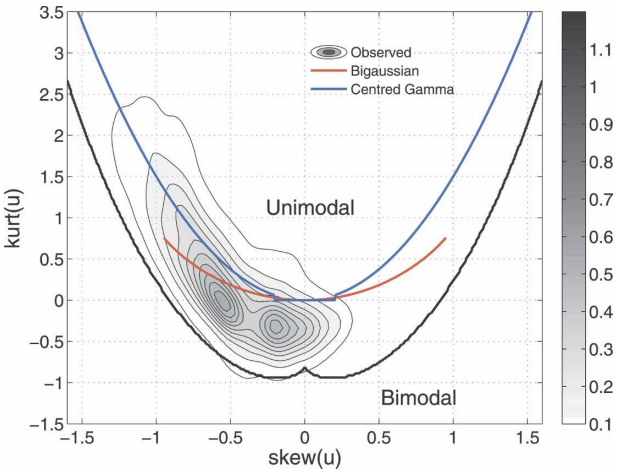

FIG. 8. Relationship between skew(u) and kurt(u). Shaded contours are the same as in Fig. 7; blue line represents the relationship for the centered gamma distribution; red line represents the relationship for the bi-Gaussian distribution. The black contour delimits the boundary between parameter ranges for which the constrained maximum entropy pdf is unimodal or bimodal.

related to skew(u); a kernel density estimate of the joint distribution of these two moments from the SeaWinds observations is presented in Fig. 8. The bi-Gaussian and centered gamma distributions also generally have nonzero kurtosis, although its value cannot be specified separately from the skewness. The relationships between skew(u) and kurt(u) for these two distributions are plotted in Fig. 8. For both of these distributions, the relationship between the skewness and kurtosis is similar to that of the observed along-mean sea surface wind component. Conversely, the relationship between moments assumed in section 4b for the Gram–Charlier and constrained maximum entropy pdfs [i.e., kurt(u) = 0] is very different from that characterizing the observations. It is therefore not surprising that the representation of the pdf of w by the bi-Gaussian and centered gamma distributions is superior to that by the Gram–Charlier and constrained maximum entropy distributions with kurt(u) equal to zero.

The fields of mean(w), std(w), and skew(w) that follow from the Gram–Charlier and constrained maximum entropy distributions using observed values of skew(u) and kurt(u) are displayed in the eighth and ninth rows of Fig. 1; the associated difference fields with the moments estimated from the SeaWinds observations are presented in the seventh and eighth rows of Fig. 6. Incorporation of kurt(u) information does not notably improve the simulation of mean(w) and std(w), but the representation of skew(w) is dramatically improved. In particular, the strong negative tropical biases in skew(w) resulting from setting kurt(w) = 0 largely

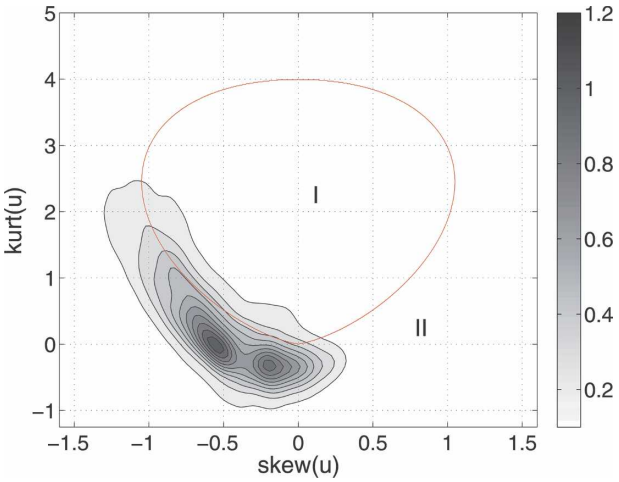

FIG. 9. Relationship between skew(u) and kurt(u). Shaded contours are the same as in Fig. 7. The red line delimits the boundary between parameter ranges where the Gram–Charlier distribution is strictly positive (region I) or takes negative values (region II).

vanish when the kurtosis information is included. The simulation is particularly good for the constrained maximum entropy distribution; the biases in simulated mean(w), std(w), and skew(w) are all very small. Similarly, the modeled relationship between moments of w is considerably improved through the inclusion of kurt(u) information (Fig. 7). For the constrained maximum entropy distribution, the scatterplot of mean(w)/std(w) with skew(w) falls almost exactly over the joint distribution estimated from the SeaWinds observations.

The character of each of the Gram–Charlier and constrained maximum entropy distributions is determined by the relative size of the skewness and kurtosis: the constrained maximum entropy pdf is unimodal for some values of the parameters and bimodal for others, and the Gram–Charlier distribution is nonnegative for some parameter values and takes negative values for others. The thick black contour in Fig. 8 delimits the boundary between unimodal and bimodal constrained maximum entropy pdfs, while the red contour in Fig. 9 denotes the border between the regions where the Gram–Charlier distribution is and is not strictly positive. The observed values of skew(u) and kurt(u) fall almost entirely within the parameter range for which the constrained maximum entropy distribution is unimodal; observed pdfs of u are generally unimodal, so spurious bimodality does not arise if both skew(u) and kurt(u) information are used in the constrained maximum entropy pdf [although it does arise if kurt(u) is fixed to be zero]. On the other hand, the observed values of skew(u) and kurt(u) fall largely outside the range in which the Gram–Charlier distribution is nonnegative (and is therefore realizable). Being both unimodal and realizable, the pdfs of u characterized by the constrained maximum entropy distribution are therefore much more realistic than those based on the Gram–Charlier expansion; it is not surprising that the representation of the pdf of w obtained from the constrained maximum entropy pdfs is superior to that obtained from the Gram–Charlier distribution.

The results presented in this section demonstrate that a highly accurate parameterization of the pdf of sea surface wind speeds (in terms of the mean, standard deviation, and skewness fields) can be developed in terms of the mean, standard deviation, skewness, and kurtosis of the along-mean sea surface wind component. Of the four non-Gaussian distributions considered, the best model followed from the constrained maximum entropy distribution. The following section will discuss the implications of these results for the development of operational parameterizations.

5. Discussion and conclusions

The distributions considered in section 4 are not on an equal footing: the Gaussian distribution requires specification of only the mean and standard deviation of the along-mean sea surface wind component u; the bi-Gaussian and centered gamma distributions require the specification of mean, standard deviation, and skewness; and the Gram–Charlier and constrained maximum entropy distributions require the specification of mean, standard deviation, skewness, and kurtosis. The superiority of the Gram–Charlier and constrained maximum entropy distributions over the Gaussian distribution in the parameterization of the pdf of sea surface wind speeds, w, is not surprising given the fact that the former take as input more information than the latter. From the perspective of practical implementations of this parameterization (e.g., calculating gridbox-averaged air/sea fluxes in a GCM), knowledge of higher-order moments of u is required. In fact, skew(u) and kurt(u) can be very well predicted by mean(u) and std(u), as boundary layer dynamics places strong constraints on the relationship between these moments [e.g., Monahan (2004a,b, 2006a); Fig. 8]. Thus, all that is needed for highly accurate parameterizations of the pdf of sea surface wind speeds in terms of gridbox-scale vector winds are the mean and standard deviation of u. The former is a standard GCM output field, and parameterizations for the latter are already in use (e.g., Cakmur et al. 2004). As the Gram–Charlier and constrained maximum entropy distributions can therefore be expressed solely in terms of mean(u) and

std(u), they can be employed in practical computations with no more information than is required by the much less accurate Gaussian parameterization [as was demonstrated for the Gram–Charlier distribution in Monahan (2006a)].

This study has extended the results of Monahan (2006a) in two primary ways. First, through consideration of the relative entropy between the observed wind speed pdf and the best-fit Weibull distribution, the degree of and spatial structure of non-Weibull behavior in sea surface wind speeds has been characterized. The strongest non-Weibull structure appears in the Tropics and subtropics, consistent with the fact that the observed relationship between the ratio mean(w)/std(w) and skew(w) deviates most from the associated relationship for a Weibull variable where skew(w) is negative (Figs. 2 and 7).

Second, empirical parameterizations of the pdf of w based on different models for the joint pdf of the sea surface vector winds have been compared. It was shown in Monahan (2006a) that incorporation of skew(u) and kurt(u) information through a Gram–Charlier distribution improved the performance of the parameterized pdf of w relative to the model assuming isotropic Gaussian fluctuations considered in Cakmur et al. (2004). In the present study, an analytic expression for the pdf of w was found for anisotropic Gaussian fluctuations in the sea surface vector wind, and it was shown that accounting for anisotropy in the fluctuations did not improve the accuracy of the parameterization of this pdf. This result reinforces the conclusion of Monahan (2006a) that the observed non-Gaussian structure in the pdf of the sea surface vector winds contributes importantly to observed structure in the pdf of w. Four different non-Gaussian models for u were then compared: two, the bi-Gaussian and centered gamma distributions, allow specification of skew(u) independently from mean(u) and std(u); two others, the Gram–Charlier and constrained maximum entropy distributions, allow the independent specification of both skew(u) and kurt(u). To first order, all four distributions provide a significantly improved representation of the pdf of w so long as the values of skew(u) and kurt(u) are related in the manner characteristic of observations. This relationship between moments is satisfied approximately by the bi-Gaussian and centered gamma distributions, but must be explicitly imposed for the Gram–Charlier and constrained maximum entropy distributions. Although to a first approximation the structure of the pdf of w is captured by all four distributions, the representation is the best for the constrained maximum entropy distribution. In an information theoretic sense, the constrained maximum entropy pdf is the least-biased distribution among all pdfs with specified moments (e.g., Jaynes 1957; Majda et al. 2005); it is interesting that this distribution provides the best representation of the pdf of u.

We have demonstrated that highly accurate parameterizations of the pdf of sea surface wind speeds can be developed in terms of the mean and standard deviation of the along-mean wind component, in association with a parameterization of the skewness and kurtosis of u in terms of the lower-order moments. This latter parameterization can be empirical (as in Monahan 2006a) or mechanistic (as in Monahan 2004b). Mechanistic parameterizations are preferable to empirical ones, particularly in the context of simulating a changing climate; however, existing mechanistic models are qualitatively accurate but quantitatively inaccurate (Monahan 2004b, 2006a). A goal of future study is the refinement of these mechanical models of the relationship between the moments of sea surface vector winds and their inclusion in parameterizations of sea surface wind speeds appropriate for use in operational climate models. It is to be anticipated that improvements to diagnosed air/sea fluxes will be most dramatic in situations when the vector winds are most variable, and will be due either to differences between the mean flux and the flux associated with the mean wind speed or to differences between the magnitude of the mean vector wind and the mean wind speed. The latter biases, characteristic of situations with strong variability in vector wind direction such as found in conditions of free convection, are the focus of gustiness parameterizations (e.g., Redelsperger et al. 2000; Williams 2001). The incorporation of buoyancy effects in the mechanistic surface wind speed parameterization presented in Monahan (2006a), in order to better represent free convective situations, is another goal of future study. Exchanges between the atmosphere and the ocean are at the heart of the coupled dynamics of the climate system; the development of improved parameterizations of surface wind pdfs is an important component of improving simulations of past, present, and future climates.

Acknowledgments. The author acknowledges support from the Natural Sciences and Engineering Research Council of Canada, from the Canadian Foundation for Climate and Atmospheric Sciences, and from the Canadian Institute for Advanced Research Earth System Evolution Program. The author would particularly like to thank Andrew Majda and John Scinocca for their valuable comments and suggestions on this work. This study was also improved by the helpful comments of three anonymous reviewers.

APPENDIX A

Wind Speed pdf for Anisotropic Gaussian Vector Winds

We assume that the winds in the along- and cross-wind directions are independent and Gaussian, with (in general) different standard deviations:

$$p(u) = \frac{1}{\sqrt{2\pi\sigma_u^2}} \exp\left[-\frac{1}{2} \frac{(u - \overline{u})^2}{\sigma_u^2} \right] \tag{A1}$$

$$p(\upsilon) = \frac{1}{\sqrt{2\pi\sigma_\upsilon^2}} \exp\left(-\frac{1}{2} \frac{\upsilon^2}{\sigma_\upsilon^2} \right), \tag{A2}$$

so the joint pdf is

$$p(u, \upsilon) = \frac{1}{2\pi\sigma_u\sigma_\upsilon} \exp\left\{ -\frac{1}{2} \left[\frac{(u - \overline{u})^2}{\sigma_u^2} + \frac{\upsilon^2}{\sigma_\upsilon^2} \right] \right\}. \tag{A3}$$

Moving to polar coordinates, $(u, \upsilon) = (w \cos\theta, w \sin\theta)$, we have

$$p(w, \theta) = \frac{w}{2\pi\sigma_u\sigma_\upsilon} \exp\left\{ -\frac{1}{2} \left[\frac{(w \cos\theta - \overline{u})^2}{\sigma_u^2} + \frac{w^2 \sin\theta}{\sigma_\upsilon^2} \right] \right\}, \tag{A4}$$

which can be rearranged as

$$p(w, \theta) = \frac{w}{2\pi\sigma_u\sigma_\upsilon} \exp\left(-\frac{w^2 + \overline{u}^2}{2\sigma_u^2} \right) \exp\left[\frac{w^2 \sin^2\theta}{2} \left(\frac{1}{\sigma_u^2} - \frac{1}{\sigma_\upsilon^2} \right) \right] \exp\left(\frac{\overline{u} w \cos\theta}{\sigma_u^2} \right), \tag{A5}$$

so

$$p(w) = \frac{w}{2\pi\sigma_u\sigma_\upsilon} \exp\left(-\frac{w^2 + \overline{u}^2}{2\sigma_u^2} \right) \int_0^{2\pi} \exp\left[\frac{w^2 \sin^2\theta}{2} \left(\frac{1}{\sigma_u^2} - \frac{1}{\sigma_\upsilon^2} \right) \right] \exp\left(\frac{\overline{u} w \cos\theta}{\sigma_u^2} \right) d\theta. \tag{A6}$$

We can obtain a power series expression for the integral by expanding the first exponential in the integrand:

$$p(w) = \frac{w}{2\pi\sigma_u\sigma_\upsilon} \exp\left(-\frac{w^2 + \overline{u}^2}{2\sigma_u^2} \right) \sum_{k=0}^{\infty} \frac{\left[\frac{w^2}{2} \left(\frac{1}{\sigma_u^2} - \frac{1}{\sigma_\upsilon^2} \right) \right]^k}{k!} \int_0^{2\pi} \sin^{2k}\theta \exp\left(\frac{\overline{u} w \cos\theta}{\sigma_u^2} \right) d\theta. \tag{A7}$$

Using the fact that

$$\int_0^{2\pi} e^{z \cos\theta} \sin^{2k}\theta \, d\theta = 2\sqrt{\pi}\Gamma(k + 1/2) \left(\frac{2}{z} \right)^k I_k(z) \tag{A8}$$

(Gradshteyn and Ryzhik 2000), where $I_k(z)$ is the associated Bessel function of the first kind, we obtain the expression Eq. (13). This series generally converges slowly (and therefore requires a large number of terms for a good approximation). Numerical computation of Eq. (13) is complicated because of the factor $\Gamma(k + 1/2)/k!$, the numerator and denominator of which grow rapidly. For larger values of k, we can use the approximation

$$\Gamma(z) \simeq \sqrt{\frac{2\pi}{z}} z^z e^{-z} \left(1 + \frac{1}{12z} \right) \tag{A9}$$

to obtain

$$\frac{\Gamma(k+1/2)}{k!} \simeq \sqrt{\frac{e}{k+1}}\left(\frac{k+1/2}{k+1}\right)^k \left[\frac{1+\frac{1}{12(k+1/2)}}{1+\frac{1}{12(k+1)}}\right] \tag{A10}$$

(an equation that is accurate to within 0.02% for $k \geq 1$).

APPENDIX B

Probability Distributions

a. Weibull distribution

A random variable x with a two-parameter Weibull distribution has the pdf

$$p_{\mathrm{wbl}}(x; a, b) = \frac{b}{a}\left(\frac{x}{a}\right)^{b-1} \exp\left[-\left(\frac{x}{a}\right)^b\right]. \tag{B1}$$

The parameters a and b are denoted, respectively, the scale and shape parameters of the distribution. Averages of powers of x are given simply by

$$\mathrm{mean}(x^k) = a^k \Gamma\left(1+\frac{k}{b}\right), \tag{B2}$$

where $\Gamma(z)$ is the gamma function. In particular, the mean, standard deviation, skewness, and kurtosis of x are given by

$$\mathrm{mean}(x) = a\Gamma\left(1+\frac{1}{b}\right) \tag{B3}$$

$$\mathrm{std}(x) = a\left[\Gamma\left(1+\frac{2}{b}\right) - \Gamma^2\left(1+\frac{1}{b}\right)\right]^{1/2} \tag{B4}$$

$$\mathrm{skew}(x) = \frac{\Gamma\left(1+\frac{3}{b}\right) - 3\Gamma\left(1+\frac{1}{b}\right)\Gamma\left(1+\frac{2}{b}\right) + 2\Gamma^3\left(1+\frac{1}{b}\right)}{\left[\Gamma\left(1+\frac{2}{b}\right) - \Gamma^2\left(1+\frac{1}{b}\right)\right]^{3/2}} \tag{B5}$$

$$\mathrm{kurt}(x) = \frac{\Gamma\left(1+\frac{4}{b}\right) - 4\Gamma\left(1+\frac{3}{b}\right)\Gamma\left(1+\frac{1}{b}\right) + 6\Gamma\left(1+\frac{2}{b}\right)\Gamma^2\left(1+\frac{1}{b}\right) - 3\Gamma^4\left(1+\frac{1}{b}\right)}{\left[\Gamma\left(1+\frac{2}{b}\right) - \Gamma^2\left(1+\frac{1}{b}\right)\right]^2} - 3. \tag{B6}$$

More complete descriptions of the Weibull distribution and the estimate of Weibull parameters from data are given in Johnson et al. (1994) and Monahan (2006a).

b. Bi-Gaussian distribution

A random variable x with a bi-Gaussian distribution has the probability density function made up of two back-to-back half Gaussian pdfs:

$$p_{\mathrm{bg}}(x;\mu,\sigma,\epsilon) = \frac{1}{\sqrt{2\pi\sigma^2}}\begin{cases} \exp\left[-\dfrac{(x-\mu)^2}{2\sigma^2(1-\epsilon)^2}\right] & x < \mu \\ \exp\left[-\dfrac{(x-\mu)^2}{2\sigma^2(1+\epsilon)^2}\right] & x > \mu. \end{cases} \tag{B7}$$

For this distribution, the quantity μ is the mode (most likely value) but not the mean. This pdf has leading moments:

$$\mathrm{mean}(x) = \mu + \sqrt{\frac{8}{\pi}}\sigma\epsilon \tag{B8}$$

$$\mathrm{std}(x) = \sigma\left[1+\left(3-\frac{8}{\pi}\right)\epsilon^2\right]^{1/2} \tag{B9}$$

$$\mathrm{skew}(x) = \sqrt{\frac{8}{\pi}}\epsilon\frac{\left[1+\left(\frac{16}{\pi}-5\right)\epsilon^2\right]}{\left[1+\left(3-\frac{8}{\pi}\right)\epsilon^2\right]^{3/2}}. \tag{B10}$$

c. Centered gamma distribution

A standardized random variable z with a centered gamma distribution has the probability density function

$$p_{\rm cg}(z;\beta) = \begin{cases} \dfrac{|\beta|}{\Gamma(\beta^2)}[\beta(z+\beta)]^{\beta^2-1} \exp[-\beta(z+\beta)] & z+\beta > 0 \\ 0 & z+\beta < 0 \end{cases} \tag{B11}$$

(e.g., Turkington et al. 2001). This distribution has moments:

$$\text{mean}(z) = 0 \tag{B12}$$

$$\text{std}(z) = 1 \tag{B13}$$

$$\text{skew}(z) = 2\beta^{-1} \tag{B14}$$

$$\text{kurt}(z) = 6\beta^{-2}. \tag{B15}$$

As $\beta \to \infty$, $p_{\rm cg}(z;\beta)$ approaches a Gaussian distribution with mean zero and unit variance. The pdf (B11) is numerically awkward for large values of β; more regular is the cumulative distribution function (cdf)

$$F_{\rm cg}(z;\beta) = \int_{-\infty}^{z} p_{\rm cg}(u;\beta)\,du = \begin{cases} \gamma(\beta^2, \beta[z+\beta]) & z+\beta > 0 \\ 0 & z+\beta < 0, \end{cases} \tag{B16}$$

where $\gamma(a, u)$ is the incomplete Gamma function

$$\gamma(a,u) = \frac{1}{\Gamma(a)}\int_0^u t^{a-1}e^{-t}\,dt \tag{B17}$$

(cf. Gradshteyn and Ryzhik 2000). Figure 10 plots $p_{\rm cg}(z;\beta)$ for representative values of γ. The random variable $x = \sigma z + \mu$ will have the centered gamma pdf

$$p_{\rm cg}(x;\beta) = \frac{1}{\sigma}p_{\rm cg}\left(\frac{x-\mu}{\sigma};\beta\right), \tag{B18}$$

with mean μ, standard deviation σ, and skewness and kurtosis given by Eqs. (B14) and (B15), respectively.

d. Gram–Charlier expansions

A standardized random variable z with the Gram–Charlier distribution

$$p_{\rm gc}(z;\nu,\kappa) = \frac{1}{\sqrt{2\pi}}\left[1 + \frac{\nu}{6}\text{He}_3(z) + \frac{\kappa}{24}\text{He}_4(z)\right]\exp\left(-\frac{z^2}{2}\right), \tag{B19}$$

where

$$\text{He}_3(z) = z^3 - 3z \tag{B20}$$

$$\text{He}_4(z) = z^4 - 6z^2 + 3 \tag{B21}$$

are Hermite polynomials of order 3 and 4 (following the notation of Gradshteyn and Ryzhik (2000, p. xxxvii), will have mean zero, standard deviation 1, skewness ν, and kurtosis κ. However, because the quantity $p_{\rm gc}(z)$ given by Eq. (B19) is not positive-definite, it is not a true probability density function (e.g., Johnson et al. 1994; Jondeau and Rockinger 2001). In particular, because the cumulative distribution function associated with (B19) is not monotonic, the associated random variable is not realizable. The Gram–Charlier distributions can be useful for producing a distribution with specified moments, but cannot generally be used to generate stochastic processes with these moments.

e. Constrained maximum entropy pdfs

Information theory defines the Shannon entropy H associated with the pdf $p(x)$ as the integral

$$H = -\int_{-\infty}^{\infty} p(x)\ln p(x)\,dx \tag{B22}$$

(e.g., Cover and Thomas 1991; Majda et al. 2005). Shannon entropy (or more simply entropy) measures the spread (or uncertainty) of a pdf. When the pdf is very narrow, so that the distribution of x is tight and the value for x is known with confidence, then H is relatively small. Conversely, when the distribution of x is broad and its value is highly uncertain, then H is relatively large. In this sense, H is a measure of how little information we have about a system. Of all pdfs with the same covariance structure, the Gaussian distribution has the maximum entropy.

Given the problem of determining a pdf $p(x)$ with specified moments

$$m_k = \int_{-\infty}^{\infty} x^k p(x)\,dx, \quad k = 1, \ldots, 2M \tag{B23}$$

but otherwise unspecified, it is sensible to calculate the pdf $p^*(x)$ that maximizes H subject to the moment constraints (B23). As H measures how little information we have about a system, this constrained maximum en-

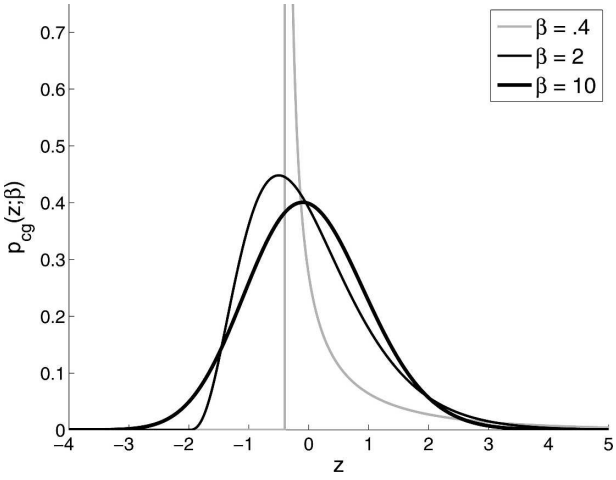

FIG. 10. Centered gamma pdfs $p_{cg}(z; \beta)$ for $\beta = 0.4$ (gray line), $\beta = 2$ (thin black line), and $\beta = 10$ (thick black line).

tropy pdf will have the least amount of information of all pdfs with the specified moments, and in this sense is the least biased pdf (Jaynes 1957). As is discussed in detail in Abramov and Majda (2004), the constrained maximum entropy pdf $p^*(x)$ takes the exponential form

$$p^*(x) = \frac{1}{Z} \exp\left(\sum_{k=1}^{2M} l_k x^k \right), \tag{B24}$$

where

$$Z = \int_{-\infty}^{\infty} \exp\left(\sum_{k=1}^{2M} l_k x^k \right) dx \tag{B25}$$

and the Lagrange multipliers l_k can be obtained from an unconstrained optimization problem, which has a unique solution because H is a concave function of p (Wu et al. 2001). Note that it is clear from the form of Eq. (B24) why an even number of moments must be used to constrain the pdf, and why l_{2M} must be negative; otherwise, the integral of $p^*(x)$ from $-\infty$ to ∞ would not be finite.

REFERENCES

Abramov, R. V., and A. J. Majda, 2004: Quantifying uncertainty for non-Gaussian ensembles in complex systems. *SIAM J. Sci. Comput.,* **26,** 411–447.

——, ——, and R. Kleeman, 2005: Information theory and predictability for low-frequency variability. *J. Atmos. Sci.,* **62,** 65–87.

Bauer, E., 1996: Characteristic frequency distributions of remotely sensed *in situ* and modelled wind speeds. *Int. J. Climatol.,* **16,** 1087–1102.

Bourassa, M. A., D. M. Legler, J. J. O'Brien, and S. R. Smith, 2003: SeaWinds validation with research vessels. *J. Geophys. Res.,* **108,** 3019, doi:10.1029/2001JC001028.

Cakmur, R., R. Miller, and O. Torres, 2004: Incorporating the effect of small-scale circulations upon dust emission in an atmospheric general circulation model. *J. Geophys. Res.,* **109,** D07201, doi:10.1029/2003JD004067.

Chelton, D. B., and M. H. Freilich, 2005: Scatterometer-based assessment of 10-m wind analyses from the operational ECMWF and NCEP numerical weather prediction models. *Mon. Wea. Rev.,* **133,** 409–429.

Conradsen, K., L. Nielsen, and L. Prahm, 1984: Review of Weibull statistics for estimation of wind speed distributions. *J. Climate Appl. Meteor.,* **23,** 1173–1183.

Cover, T. M., and J. A. Thomas, 1991: *Elements of Information Theory.* Wiley, 542 pp.

Deaves, D., and I. Lines, 1997: On the fitting of low mean windspeed data to the Weibull distribution. *J. Wind Eng. Ind. Aerodyn.,* **66,** 169–178.

Ebuchi, N., H. C. Graber, and M. J. Caruso, 2002: Evaluation of wind vectors observed by QuikSCAT/SeaWinds using ocean buoy data. *J. Atmos. Oceanic Technol.,* **19,** 2049–2062.

Erickson, D. J., and J. A. Taylor, 1989: Non-Weibull behavior observed in a model-generated global surface wind field frequency distribution. *J. Geophys. Res.,* **94,** 12 693–12 698.

Gradshteyn, I., and I. Ryzhik, 2000: *Table of Integrals, Series, and Products.* 6th ed. Academic Press, 1163 pp. (Translated from Russian by Scripta Technica, Inc.)

Haven, K., A. Majda, and R. Abramov, 2005: Quantifying predictability through information theory: Small sample estimation in a non-Gaussian framework. *J. Comput. Phys.,* **206,** 334–362.

Hennessey, J. P., 1977: Some aspects of wind power statistics. *J. Appl. Meteor.,* **16,** 119–128.

Isemer, H.-J., and L. Hasse, 1991: The scientific Beaufort equivalent scale: Effects on wind statistics and climatological air-sea flux estimates in the North Atlantic Ocean. *J. Climate,* **4,** 819–836.

Jaynes, E., 1957: Information theory and statistical mechanics. *Phys. Rev.,* **106,** 620–630.

Jet Propulsion Laboratory, 2001: SeaWinds on QuikSCAT Level 3: Daily, gridded ocean wind vectors. Tech. Rep. JPL PO.DAAC Product 109, California Institute of Technology, 39 pp. [Available online at http://podaac.jpl.nasa.gov/pub/ocean_wind/quikscat/L3/doc/qscat_L3.doc.]

Johnson, N., S. Kotz, and N. Balakrishnan, 1994: *Continuous Univariate Distributions.* Vol. 1. Wiley, 756 pp.

Jondeau, E., and M. Rockinger, 2001: Gram–Charlier densities. *J. Econ. Dyn. Control,* **25,** 1457–1483.

Justus, C., W. Hargraves, A. Mikhail, and D. Graber, 1978: Methods for estimating wind speed frequency distributions. *J. Appl. Meteor.,* **17,** 350–353.

Kleeman, R., 2002: Measuring dynamical prediction utility using relative entropy. *J. Atmos. Sci.,* **59,** 2057–2072.

——, 2007: Statistical predictability in the atmosphere and other dynamical systems. *Physica D,* **230,** 65–71.

——, and A. Majda, 2005: Predictability in a model of geophysical turbulence. *J. Atmos. Sci.,* **62,** 2864–2879.

Mahrt, L., and J. Sun, 1995: The subgrid velocity scale in the bulk aerodynamic relationship for spatially averaged scalar fluxes. *Mon. Wea. Rev.,* **123,** 3032–3041.

Majda, A. J., R. V. Abramov, and M. J. Grote, 2005: *Information Theory and Stochastics for Multiscale Nonlinear Systems.* Amer. Math. Soc., 133 pp.

Monahan, A. H., 2004a: Low-frequency variability of the statistical moments of sea surface winds. *Geophys. Res. Lett.,* **31,** L10302, doi:10.1029/2004GL019599.

——, 2004b: A simple model for the skewness of global sea surface winds. *J. Atmos. Sci.,* **61,** 2037–2049.

——, 2006a: The probability distribution of sea surface wind speeds. Part I: Theory and SeaWinds observations. *J. Climate,* **19,** 497–520.

——, 2006b: The probability distribution of sea surface wind speeds. Part II: Dataset intercomparison and seasonal variability. *J. Climate,* **19,** 521–534.

Pang, W.-K., J. J. Forster, and M. D. Troutt, 2001: Estimation of wind speed distribution using Markov chain Monte Carlo techniques. *J. Appl. Meteor.,* **40,** 1476–1484.

Pavia, E. G., and J. J. O'Brien, 1986: Weibull statistics of wind speed over the ocean. *J. Climate Appl. Meteor.,* **25,** 1324–1332.

Redelsperger, J.-L., F. Guichard, and S. Mondon, 2000: A parameterization of mesoscale enhancement of surface fluxes for large-scale models. *J. Climate,* **13,** 402–421.

Silverman, B. W., 1986: *Density Estimation for Statistics and Data Analysis.* Chapman and Hall, 175 pp.

Stewart, D. A., and O. M. Essenwanger, 1978: Frequency distribution of wind speed near the surface. *J. Appl. Meteor.,* **17,** 1633–1642.

Takle, E., and J. Brown, 1978: Note on the use of Weibull statistics to characterize wind-speed data. *J. Appl. Meteor.,* **17,** 556–559.

Taylor, P. K., Ed., 2000: Intercomparison and validation of ocean-atmosphere energy flux fields. Joint WCRP/SCOR Working Group on Air-Sea Fluxes Final Rep. WMO/TD 1036, 306 pp.

Tuller, S. E., and A. C. Brett, 1984: The characteristics of wind velocity that favor the fitting of a Weibull distribution in wind speed analysis. *J. Climate Appl. Meteor.,* **23,** 124–134.

Turkington, B., A. Majda, K. Haven, and M. DiBattista, 2001: Statistical equilibrium predictions of jets and spots on Jupiter. *Proc. Natl. Acad. Sci. USA,* **98,** 12 346–12 350.

Wanninkhof, R., 1992: Relationship between wind speed and gas exchange over the ocean. *J. Geophys. Res.,* **97,** 7373–7382.

——, and W. R. McGillis, 1999: A cubic relationship between air-sea CO_2 exchange and wind speed. *Geophys. Res. Lett.,* **26,** 1889–1892.

——, S. C. Doney, T. Takahashi, and W. R. McGillis, 2002: The effect of using time-averaged winds on regional air-sea CO_2 fluxes. *Gas Transfer at Water Surfaces, Geophys. Monogr.,* Vol. 127, Amer. Geophys. Union, 351–356.

Williams, A. G., 2001: A physically based parameterization for surface flux enhancement by gustiness effects in dry and precipitating convection. *Quart. J. Roy. Meteor. Soc.,* **127,** 469–491.

Wu, Z., G. N. Phillips, R. Tapia, and Y. Zhang, 2001: A fast Newton algorithm for entropy maximization in phase determination. *SIAM Rev.,* **43,** 623–642.